Model for Temperature Profiles in Large Diameter Electrochromatography Columns

Craig Keim
Laboratory of Renewable Resources Engineering and Dept. of Agricultural and Biological Engineering, Purdue University, West Lafayette, IN 47907
and
Lincoln Laboratory, Massachusetts Institute of Technology, Lexington, MA 02420

Michael Ladisch
Laboratory of Renewable Resources Engineering, Dept. of Agricultural and Biological Engineering, and Dept. of Biomedical Engineering, Purdue University, West Lafayette, IN 47907

Scale-up of electrochromatographic separations has been problematic due to electrically induced heating. A two-dimensional transient temperature model for electrochromatography was developed, which accounts for physical properties of the stationary and mobile phase, and the column wall. The model also accounts for both the temperature effect on the electrical conductivity and a nonuniform, radially variant current density. This model was compared to experimental data from two electrochromatography systems with different cylindrical-column dimensions, packing materials, and operating conditions. In all cases, the model predicts the temperature to within 3°C of the actual temperature, both for column heatup and cooldown. Separation of a mixture of model proteins on the 3.81-cm-ID scale was used as the basis for scale-up calculations. The model identifies equipment parameters that control heating characteristics and can be scaled up to process 75 mL of sample per run.

Introduction

Separations based on electrokinetic phenomena have become more common over the past decade, particularly in the analytical realm. Techniques such as gel electrophoresis and capillary electrophoresis are commonly used in analyzing biological and pharmaceutical products. While these techniques often offer superior resolution over chromatography, scale-up from analytical to preparative-sized separations has been problematic due to electrically induced heating in these devices. One electrokinetic technique that has scale-up potential is electrochromatography, which combines an axial electric field with chromatographic packing (Rudge et al., 1993; Basak and Ladisch, 1995; Basak et al., 1995; Cole and Cabezas, 1995).

Correspondence concerning this article should be addressed to M. Ladisch.

To date, electrochromatography research has been primarily devoted to columns that were 1.5 cm ID or smaller that used cooling jackets to dissipate electrically induced heating. Larger diameter columns suffer from reduced heat removal through the cooling jacket due to a decreased surface-area-to-volume ratio. Different approaches for controlling the temperature in the column can be used. For example, reducing the conductivity of the mobile and stationary phase reduces joule heating (Basak et al., 1994).

Research on electrochromatography column design and operation requires quantitative metrics by which column temperature as a function of position and time can be modeled and ultimately predicted. We developed a means of measuring the temperature inside the column without disrupting the flow patterns or electric field (Keim and Ladisch, 2000). Since the temperature profile in the column can be measured,

Table 1. Electrophoretic Modeling Conditions Available in the Literature

	Transient (T) or Steady State (S)	Coordinate System Cylind. (C) or Rectang. (R)	No. of Dimensions	Wall Heat Transfer Const. (C) or Variable (V)	Temp. Variation of Conductivity	Accounts for Fluid Flow	Temp. Variation of Physical Const.	Comparsion to Exp. Data	Accounts for Stationary Phase Properties	Accounts for Variable Current Density
This work (2002)	T	C	2	V	√	√	√	√	√	√
Raj (1994)	S	C	2	C	√	√	√			
Raj and Hunter (1991)	S	C	2	C	√	√				
Ivory and Gobie (1990)	S	C	1	C	√					
Turk and Ivory (1984)	S	R	3	C		√				
Lynch and Saville (1981)		R	3	C	√	√				
Ostrach (1977)	S	R	3	C		√				
Tiselius (1937)	S	R	1	C						
Capillary electrophoresis										
Bello and Righetti (1992)	S/T	C	1		√					
Gobie and Ivory (1990)	S	C	1	V	√					
Grushka et al. (1989)	S	C	1	V	√					

mathematical models of electrochromatography can now be validated with the experimental data.

Models for steady-state heating effects in electrophoretic separations have been available in the literature for over 60 years. Table 1 summarizes model assumptions, the coordinate systems, and numbers of spatial dimensions of models presented in the literature. With few exceptions, steady-state operating conditions are assumed for modeling purposes.

Ivory and Gobie (1990) account for radial conductive heat transfer at constant-temperature column wall. Using Eq. 1, they estimated the steady-state radial temperature rise in the column for a given voltage gradient and current density

$$T_r - T_w = \frac{i_T\left(\frac{d\Phi}{dx}\right)R^2}{4k_f}\left[1-\left(\frac{r}{R}\right)^2\right], \qquad (1)$$

where T_r is the temperature at any radial position, r, T_w is the temperature of the column wall, i_T is the total current density, $d\Phi/dx$ is the voltage gradient, R is the column radius, and k_f is the thermal conductivity of the fluid in the packed bed. Ivory and Goby (1990) found that a 40°C temperature rise will occur at a tube diameter of 2 to 3 mm for a 100-V/cm voltage gradient [for $k_f = 0.5$ W/(m·°C]. Equation 1 predicts that an increase in column diameter from 1.5 cm to 5.1 cm will result in a temperature that is 11.56 times the temperature rise of the 1.5-cm column. However, large voltage gradients are not always needed, particularly for process scale separations, where resolution of the components into only two or three peaks is needed. Scale-up of the system depends on using a lower voltage gradient, low conductivity buffer, and operating the column at transient conditions. This was recently demonstrated for a 3.8-cm-ID column that gave baseline separation of bovine serum albumin (BSA) and myoglobin (Keim and Ladisch, 2000). Further data and a new mathematical model are presented here for 3.81-cm-ID and 5.1-cm-ID columns at transient operation for voltage gradients from 10 V/cm to 25 V/cm.

Equipment and Stationary Phases

A complete description of the equipment used for the electrochromatography experiments is presented in Keim and Ladisch (2000). The following is a synopsis of that work. Two plexiglass columns of different dimensions were used for experimental and modeling purposes. The first column was a 5.1-cm-ID × 20.3-cm-long column and a 0.635-cm wall thickness. It was packed with Sephadex G-50 Fine (Pharmacia, Piscataway, NJ). The second column consisted of a 3.81-cm-ID × 38.1-cm-long column packed with TosoHaas HW40-C stationary phase (10,000 MW cutoff), a gift from TosoHaas (Montgomeryville, PA). The wall thickness of the second column was 1.27 cm.

The electrodes are separated from the packed bed using either an ultrafiltration membrane or a polyacrylamide gel plug. The stationary phase was retained in the column by a glass frit at either end of the packed bed. Platinum mesh, instead of individual platinum wires, were used as the electrodes to reduce current density and thereby reduce bubble formation from electrolysis gases. Electrical current was supplied by an EC650 DC power supply made by EC Apparatus Company (St. Petersburg, FL). Four Type-T thermocouples from Omega Engineering, Inc. (Stanford, CT) were spaced evenly along the axial length of both columns. Each thermocouple was inside of an electrically insulated sheath and was positioned in the radial center of the column. To achieve online detection of the proteins, the absorbance at 280 nm was obtained using a Type 6 optical unit and UA-5 recorder from Isco (Lincoln, NE). The temperatures from the four thermocouples and UV absorbance were recorded using an

IOTech/Strawberry Tree (Cleveland, OH) data-acquisition system at 8-s intervals. Both temperature and absorbance data were transferred to Microsoft Excel (Redmond, WA) for data analysis and modeling.

The mobile phase was a 3.9-mM tris[hydroxyamino]methane (tris)- 47-mM glycine, pH 8.2 solution and was selected due to its relatively low conductivity (Basak and Ladisch, 1995; Basak et al., 1994; Rudge et al., 1993). The buffer was cooled prior to entering the column using a series of cooling coils that were immersed in an ice bath. The proteins used in these studies were bovine serum albumin (A-6003, 95+% purity) and horse heart myoglobin (M-0630, 95–100% purity) from Sigma (St. Louis, MO). Void fractions were measured using BSA (MW = 68 kD) and myoglobin (MW = 17.5 kD). Both of these proteins have molecular weights that are higher than the molecular weight cutoff of the stationary phase (10 kD). The ice bath, column, detector, and fraction collector were inside of a Kelvinator refrigerated cold box. The temperature inside of the cold box was maintained between 6 and 10°C.

Modeling

Two-dimensional unsteady-state heat-transfer model

The model divides the electrochromatography column into two distinct subsystems (Figure 1). The fluid and stationary phases form the first subsystem, with axial boundaries consisting of the column inlet and outlet. The outer radial boundary of the first subsystem is the column wall and is subject to the constraint of forced convection heat transfer. The second subsystem is the column wall itself. Since the main equipment used to gather experimental data has a wall thickness of 1.27 cm, the column wall cannot be ignored in determining the heat-transfer characteristics of the column. For modeling purposes, the second subsystem is subject to forced convection on the inner surface, free convection on the outer surface, and conduction through the solid wall.

Subsystem 1. If thermal equilibrium between the mobile and stationary phases is assumed, the heat-transfer model is significantly simplified. Equation 2 accounts for mobile-phase flow, internal heat generation, and external cooling in the packed bed (Bejan, 1995).

$$\frac{\partial T}{\partial t} = \left(\frac{\alpha}{\sigma}\right)\frac{\partial^2 T}{\partial x^2} - \left(\frac{u}{\sigma}\right)\frac{\partial T}{\partial x} + \left(\frac{\alpha}{\sigma}\right)\left(\frac{1}{r}\frac{\partial}{\partial r}\left(r\frac{\partial T}{\partial r}\right)\right) + \left(\frac{\alpha}{\sigma}\right)\left(\frac{\left(\frac{\partial \Phi}{\partial x}\right)^2 \sigma_m}{k_m}\right). \quad (2)$$

In Eq. 2, T is temperature at radial position, r, and axial position, x; t is time; α is the thermal diffusivity as defined in Eq. 3; σ is the thermal capacity factor as defined in Eq. 4; u is the superficial velocity; σ_m is the electrical conductivity of the packed bed; and k_m is the thermal conductivity of the medium

$$\alpha = \frac{k_m}{\rho_f c_{p,f}} \quad (3)$$

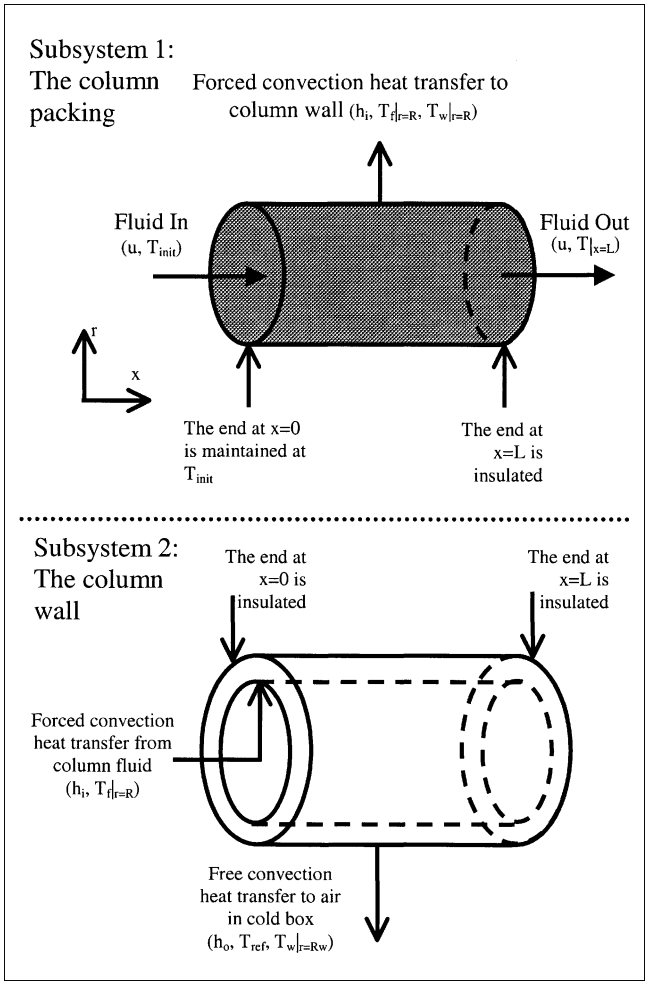

Figure 1. System for modeling with description of boundary conditions.

$$\sigma = \frac{\epsilon_T \rho_f c_{p,f} + (1-\epsilon_T)\rho_s c_{p,s}}{\rho_f c_{p,f}}. \quad (4)$$

In Eqs. 3 and 4, ρ_f is the fluid density; $c_{p,f}$ is the fluid heat capacity; ϵ_T is the total column void fraction; ρ_s is the stationary phase density; and $c_{p,s}$ is the heat capacity of stationary phase.

The following boundary conditions were used

$$T|_{x=0,r} = T_{\text{init}} \qquad \left.\frac{\partial T}{\partial x}\right|_{x=L} = 0, \qquad \left.\frac{\partial T}{\partial r}\right|_{r=0} = 0,$$

$$\text{and} \qquad k_m \left.\frac{\partial T}{\partial r}\right|_{r=R} = h_i(T_w - T), \quad (5)$$

where L is the length of the column, T_{init} is the initial temperature, and h_i is the internal heat-transfer coefficient between the column wall and the medium. The following initial

Table 2. Temperature Dependence of Physical Constants for Modeling

Physical Property	Fit of Data to Equation	R^2	Fitted Range (°C)
Water			
Density (kg/m^3)	$-4.01\times10^{-3}T^2-0.0367T+1002$	0.999	0–80
Heat capacity [kJ/(kg°C)]	$-2.75\times10^{-7}T^3+5.184\times10^{-5}T^2-2.655\times10^{-3}T+4.218$	0.994	0–80
Thermal conduct. [W/(m·K)]	$-1.143\times10^{-5}T^2+2.344\times10^{-3}T+0.5529$	0.999	0–80
Kinematic visc. (m^2/s)	$2.686\times10^{-10}T^2-3.837\times10^{-8}T+1.749\times10^{-6}$	0.989	0–80
Air			
Density (kg/m^3)	$3.78\times10^{-5}T^2-6.46\times10^{-3}T+1.20$	0.981	−170 to 125
Thermal conduct. [W/(m·K)]	$-3.61\times10^{-8}T^2+7.97\times10^{-5}T+2.41\times10^{-2}$	1.000	−170 to 125
Thermal diffus. (m^2/s)	$2.42\times10^{-10}T^2+1.29\times10^{-7}T+1.78\times10^{-5}$	0.995	−170 to 125
Kinematic vis. (m^2/s)	$1.14\times10^{-10}T^2+8.68\times10^{-8}T+1.33\times10^{-5}$	0.996	−170 to 125

Note: All equations were based on polynomial fits of data from Ozisik (1985); R^2 values for each of the polynomial fits are given in the table.

condition was used:

$$T_{(x,\,r,\,t=0)}=T_{\text{init}}. \tag{6}$$

Physical properties for the buffer and air as a function of temperature are given in Table 2.

Subsystem 2. The temperature distribution in the wall is calculated by Eqs. 7 through 9. Physical properties for modeling temperature distribution in the column wall are given in Table 3.

$$\frac{\partial T}{\partial t}=\alpha_w\left\{\frac{\partial^2 T}{\partial x^2}+\left[\frac{1}{r}\frac{\partial}{\partial r}\left(r\frac{\partial T}{\partial r}\right)\right]\right\} \tag{7}$$

$$\alpha_w=\frac{k_w}{\rho_w c_{p,w}}, \tag{8}$$

where k_w is the thermal conductivity of the column wall, ρ_w is the density of the column wall, and $c_{p,w}$ is the heat capacity of the column wall. The following boundary conditions were used

$$\left.\frac{\partial T}{\partial x}\right|_{x=0}=0,\qquad \left.\frac{\partial T}{\partial x}\right|_{x=L}=0,$$

$$k_w\left.\frac{\partial T}{\partial r}\right|_{r=R}=h_i\left(T_w-T_f\right)\big|_{r=R},$$

$$-k_w\left.\frac{\partial T}{\partial r}\right|_{r=R_w}=h_o\left(T_w-T_{\text{ref}}\right)\big|_{r=R_w}, \tag{9}$$

Table 3. Physical Constants Used for Modeling HW40-C and Plexiglass Wall

Physical Property	Value	Reference
Density (kg/m^3)	1,190	*Int. Plastic Selector* (1989)
Heat capacity [kJ/(kg·C)]	1,380	Krevelen (1976)
Thermal conduct. [(W/(m·K)]	0.0737	Int. Plastics Selector (1989)

where T_f is the mean film temperature at the inner column wall, h_o is the outside heat-transfer coefficient between the column wall and the refrigerated air, T_{ref} is the temperature of the refrigerated air, and R_w is the outside diameter of the column wall.

The equations for both subsystems were combined and solved by an alternating direction implicit solution (Vermuri and Karplus, 1981) using Visual Basic for Applications in Microsoft Excel. Model predictions were output directly to the Excel spreadsheet and compared to experimental data obtained from the data-acquisition system.

Void fraction, Reynolds number, friction factor, and pressure drop

The extraparticulate void fraction, ϵ_b, can be estimated *a priori* using Eq. 10 (Fand and Thinakaran, 1990) if the column diameter, D, and the stationary phase particle diameter, d_p, are known

$$\epsilon_b=\frac{0.151}{\left(D/d_p-1\right)}+0.360. \tag{10}$$

The calculated result is consistent with measurements made in our laboratory using large molecular-weight probes to determine the extraparticulate void fraction. The column Reynolds number, Re_D, can be calculated from Eq. 11 (Fand and Thinakaran, 1990):

$$Re_D=\frac{uD}{\nu}, \tag{11}$$

where ν is the kinematic fluid viscosity (viscosity divided by density). The particle Reynolds number, Re_d, can be calculated from Eq. 12 (Fand and Thinakaran, 1990):

$$Re_d=\frac{ud_p}{\nu}. \tag{12}$$

If Re_d is between 10^{-5} and 2.3, the fluid flow is in the Darcy region (Varahasamy and Fand, 1996). In cases where the ra-

tio of the column diameter to the particle diameter is small, it is necessary to account for wall effects in the equations for friction factor and Reynolds number. A wall correction factor term, M, must be calculated to determine the wall modified friction factor and Reynolds number using Eq. 13 (Varahasamy and Fand, 1996)

$$M = 1 + \frac{2d_p}{3D(1+\epsilon_b)}. \tag{13}$$

The modified wall-corrected, particle Reynolds number, Re_w, is calculated using Eq. 14

$$Re_w = \frac{ud_p}{\nu(1-\epsilon_b)M}. \tag{14}$$

For flows in the Darcy region, the modified, wall-corrected friction factor, f_w, can be calculated using Eq. 15

$$f_w = \frac{36\kappa}{Re_w M^2}. \tag{15}$$

The quantity κ is the wall-corrected Kozeny–Carman factor and is calculated from the following equation (Fand and Thinakaran, 1990)

$$\kappa = 5.340 - 0.6545e^{-0.09034(D/d_p)} \tag{16}$$

For D/d_p ratios exceeding 40, the Kozeny–Carman factor is equivalent to 5.34.

Stationary phase electrical conductivity

In a packed column, the voltage gradient can be estimated from Eq. 17

$$\frac{d\Phi}{dx} = \frac{i_T}{\sigma_m}. \tag{17}$$

When electrical current is passed through any medium, Joule heat is generated in the medium. The power generation per unit volume Q can be estimated from Eq. 18

$$Q = i_T\frac{d\Phi}{dx} = \left(\frac{d\Phi}{dx}\right)^2\sigma_m. \tag{18}$$

Temperature Dependence of Electrical Conductivity. The electrical conductivity of the packed bed increases with increasing temperature, ionic strength, and dissolved gasses. For all experimental runs, the ionic strength of the buffer was kept constant. Prior to each run, the buffer was either degassed using a vacuum flask or an in-line degasser placed on the inlet side of the pump. The effect of temperature on the conductivity was estimated from voltage drop and temperature measurements in the column. The model uses conductivities calculated from Eq. 19 for temperatures between 6 and 24°C and Eq. 20 for all other temperatures. For 6°C $\le T \le$ 24°C

$$\sigma_m = (-0.00203T^4 + 0.11302T^3 - 2.13578T^2 + 19.07746T + 0.39533)10^{(-4)}. \tag{19}$$

For all other temperatures,

$$\sigma_m = (3.51201T + 35.6456)10^{(-4)}. \tag{20}$$

The temperature from the previous time step at the same axial and radial position was used to calculate the conductivity for the current time step. The pK_a of the buffer, and therefore pH, is a function of temperature, which in turn will affect the local electrophoretic mobility of a protein. As described later in this article, the radial temperature profile is estimated to be on the order of 2°C to 3°C, resulting in a small gradient in the pK_a of the buffer. This in turn could contribute to peak dispersion, if the sample volume containing the protein is at this part of the column when the temperature rise occurs. Equations 19 and 20 experimentally average this effect, if present, since the effect of temperature on conductivity was estimated from measurements in the column, which by definition reflects these effects, if they are occurring.

Calculating the Voltage Drop for Constant-Current Experiments. The modeling of constant-voltage operation is simpler than the modeling of constant-current operation. Under constant-voltage operation, the heating per unit volume at any point can be calculated using Eq. 18 without having to know the local current density, assuming the electrical conductivity is known. However, under constant-current operation, the voltage gradient as well as the local current density are unknown. Since the column temperature varies radially, the electrical conductivity varies radially. The radial middle of the column has a higher conductivity and will conduct more electricity than the outer edges of the column where the conductivity is lower.

To estimate the voltage gradient across an axial length of Δx, the following rationale was used. The sum of the individual current densities multiplied by their respective areas give the total current. The current density at any given point can be calculated from the voltage gradient multiplied by the local electrical conductivity. The voltage drop at each axial location was calculated by dividing the total current by the sum of the average conductivities multiplied by their respective areas via Eq. 21.

$$\frac{\partial\Phi}{\partial x} = \frac{I}{\pi\sum_{j=1}^{j=(R/\Delta r)}\left((j\Delta r)^2 - ((j-1)\Delta r)^2\right)\left(\frac{\sigma_m|_{(x,j)} + \sigma_m|_{(x,j-1)}}{2}\right)}. \tag{21}$$

Calculation of heat-transfer coefficients

Forced-Convection Heat Transfer in a Packed Bed. Based on the analysis by Varahasamy and Fand (1996), the Nusselt number for forced-convection heat transfer in a packed bed with heat removal at the walls can be calculated from Eq. 22

$$Nu_{\text{forced}} = 0.5016 Re_D^{0.5} Pr_m^{0.4067} (f_w Re_w)^{0.1912} \left(\arctan\left(\frac{D}{d_p}\right)^{0.5}\right)^{0.9117}, \quad (22)$$

where

$$\text{Pr}_m = \frac{\nu \rho_f c_{p,f}}{k_m} = \text{Prandtl number of the media} \quad (23)$$

The value of k_m is calculated by Krupiczka (1967) as follows

$$k_m = k_f \left(\frac{k_f}{k_s}\right)^{-[0.280 - 0.757 \log_{10} \epsilon_T + 0.057 \log_{10}(k_f/k_s)]} \quad (24)$$

where k_f is the fluid thermal conductivity and k_s is the stationary-phase thermal conductivity. Once the Nusselt number has been calculated the inner heat-transfer coefficient can be calculated from Eq. 25

$$h_i = \frac{k_m Nu_{\text{forced}}}{D}. \quad (25)$$

Free-Convection Heat Transfer on the Column Wall. The Rayleigh number, Ra_D, determines the onset of natural convection. For a horizontal cylinder of diameter, D, it can be calculated from the following equation (Ozisik, 1985)

$$Ra_D = \frac{gD^3\beta(T_w - T_{\text{ref}})}{\nu^2} Pr_a, \quad (26)$$

where g is the gravitational constant, Pr_a is the Prandtl number for air at the film temperature, and β is the coefficient of thermal expansion. When Ra_D is between 10^4 and 10^7, the Nusselt number for free convection, Nu_{free}, can be evaluated from Eq. 27 (Ozisik, 1985)

$$Nu_{\text{free}} = 0.480 Ra_D^{0.250}. \quad (27)$$

Once the free-convection Nusselt number is calculated, the outer heat-transfer coefficient, h_o, can be calculated from Eq. 28

$$h_o = \frac{k_w Nu_{\text{free}}}{D} \quad (28)$$

Results and Discussion

The solution of Eqs. 2 to 28 gave the transient profiles in Figure 2A for a 3.81-cm × 38.1-cm column at the conditions indicated in the figure legend. The corresponding separation

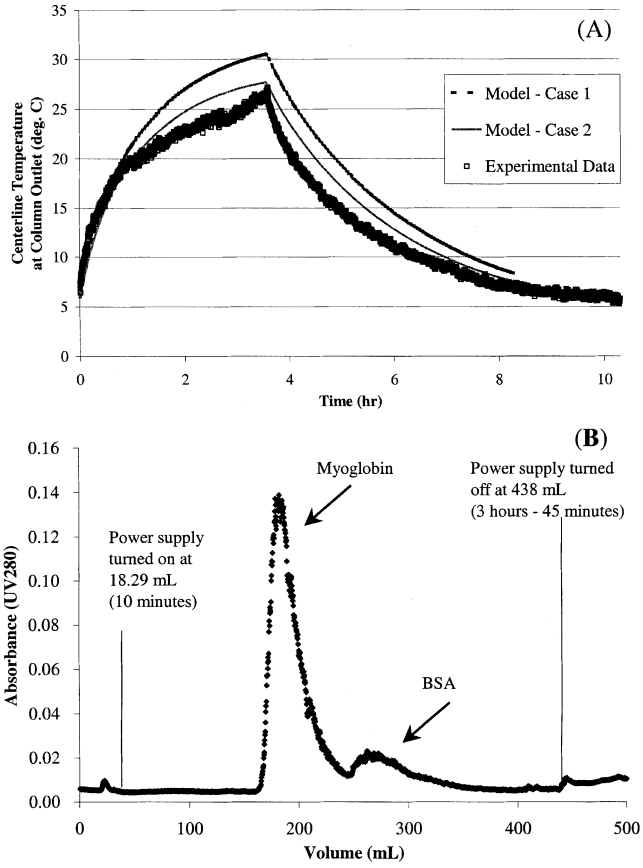

Figure 2. (A) Model vs. experimental data and (B) electrochromatographic separation of BSA and myoglobin in a 3.81cm ID × 38.1cm long column packed with TosoHaas HW-40C.

Figure 2A. Data for the radial center of the column 38.1 cm from the inlet; time step for modeling, 20 s; radial column step, 1.905 mm; radial step for column wall, 0.635 mm; mobile phase, 3.9 mM tris-47 mM glycine; flow rate, 1.951mL/min for both modeling and experimental data. Electric field was turned on at 15.3mA for 3 h and 35 min.; cold box temperature, 6°C; inlet mobile phase temperature, 2°C for both sets of data. Physical properties of water were assumed to be constant. Bulk void fraction calculated was 0.360 and total void fraction was 0.914. Model Case 1 assumes $c_{p,s}$, ρ_s, and k_s are the same as that as plexiglass; Model Case 2 assumes $c_{p,s}$, ρ_s, and k_s are the same as for water. Values of these parameters are in Tables 2 and 3. Figure 2B. Power supply was turned on at 10 min with a current of 15.3mA and turned off after 3 h and 45 min. All conditions identical to Figure 2(A). Sample size was 9.5mL of 1.048 mg/mL myoglobin and 1.144 mg/mL BSA.

is shown in Figure 2B. Since the stationary phase is a methacrylate-based resin, the heat capacity, thermal conductivity, and density were assumed to be similar to that of plexiglass (which is a methacrylate polymer), as given in Table 3. The predicted (labeled as Model Case 1 in Figure 2(a)) and experimental temperature profile at the column outlet did not coincide as closely as when the physical properties of water were used to represent the entire packed bed in a second calculation. The stationary-phase particles are porous and consist of at least 60% water by weight and the total void fraction for the packed bed is 0.914 ± 0.004. Hence, the use of the properties of water is justified. The profiles for simula-

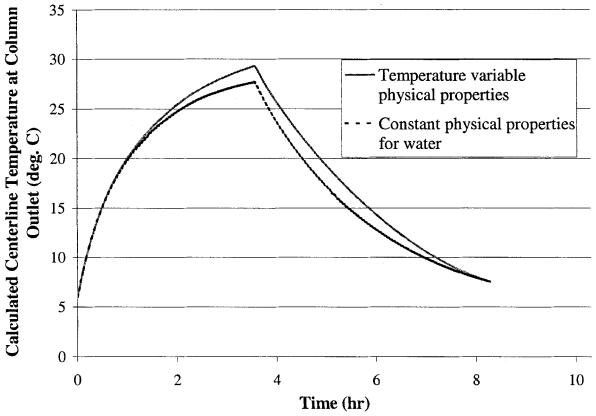

Figure 3. Difference in predicted temperatures between using constant physical properties and temperature variant physical properties of water at the column outlet.

Conditions are identical to those in Figure 2(A).

tions based on temperature-variant properties of water are similar to those for the temperature-invariant case (Figure 3). Temperature-invariant thermal properties were used, since computing time decreased from 2 h to 6 min per simulation. The model was compared to experimental data from another chromatography system that had different dimensions (5.1 × 20.3 cm) and packing material (Sephadex G-50) (Figure 4). The measured and predicted temperature rises were within 2°C.

The prediction of the temperature profile at the inlet coincided with measured temperatures for the first hour, but then diverged (Figure 5). Heating in the inlet glass frit is probably the cause. Since the porosity of the glass frit is low, the cross-sectional area for current flow is low. Thus, both the current density and the electrical resistance in the glass frit are high. High current density and high resistance result in high heating per unit volume. Thus the glass frit and the fluid it contains heats up more rapidly than the stationary phase in

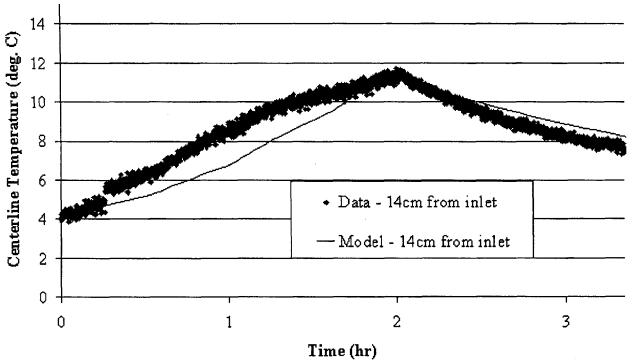

Figure 4. This model vs. another chromatographic system.

The column used for the data was 5.1 cm ID × 20.3 cm long packed with Sephadex G-50. Wall thickness was 0.635 cm. Electric current was adjusted to maintain ~10 V/cm and fluid flow rate was 0 mL/min until ~7,000 s and then electric field was turned off and pump was started at ~1.2 mL/min.

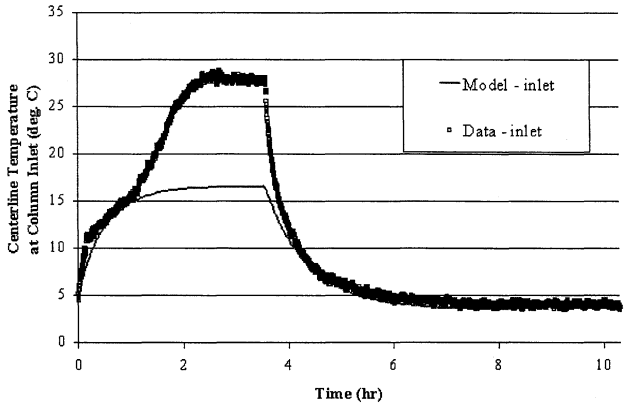

Figure 5. Experimental data at the column inlet vs. the model.

Conditions identical to those in Figure 2(A).

the rest of the column. The part of the column that is hottest to the touch is in the area where the frit touches the column wall. When the electric field is turned off, the temperature at the inlet decreases much more rapidly than the temperature at the middle and outlet thermocouples. Conversely, the temperatures at these locations do not increase until several hours after the inlet temperature rises (compare Figures 2A and 5).

A major contributor to the column temperature rise is resistance to heat transfer through the column walls. The column wall is thick, has a low thermal conductivity, and acts as a thermal insulator. While the radial temperature drop in the column is less than 3°C, the temperature drop across the column wall is over 15°C (Figure 6). If the column wall was made of a more thermally conductive material and consisted of a cooling jacket with circulating water, the temperature rise could be reduced by 50% (compare Figures 2A and 7). The experiments reported in this work were carried out in plexiglass columns instead of metal columns due to the need to select a material that was readily available and would serve as an electrical insulator. Future work should seek informa-

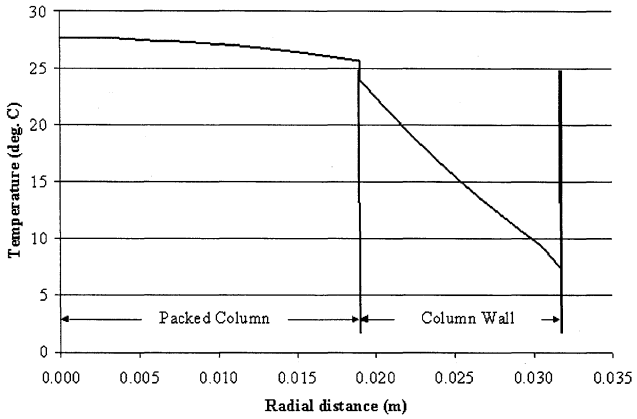

Figure 6. Predicted radial temperature at the column outlet for both the packed column and column wall immediately prior to turning off the electric field.

Conditions identical to those in Figure 2(A).

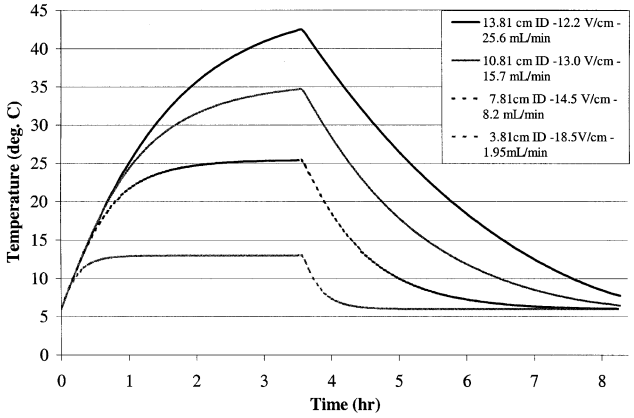

Figure 7. Predicted effect of column diameter on transient temperature rise in a column packed with HW40-C.

Column was scaled up on constant current density and constant linear velocity. Column length was 38.1 cm for all columns. Column wall was maintained at 6°C and 3.9 mM tris-47 mM glycine mobile phase was cooled to 2°C. The flow rates increase with increasing column diameter and result in a constant interstitial velocity of 7.92×10^{-5} m/s. The voltage gradients were time-averaged over the time while the electric field was applied.

tion on materials that are both thermal conductors and electrical insulators.

Temperature profiles can be calculated assuming that the stationary phase has the same heat capacity, density, and thermal conductivity as water (that is, the aqueous buffer). However, it should be noted that the effect of the stationary phase on electrical conductivity cannot be ignored. The predicted temperature rise is substantially different from experimental data if the electrical conductivity of the stationary phase is assumed to be constant. When the conductivity of the stationary phase as a function of temperature is measured and used in the model, the predicted voltage drop at the outlet is within 2 V/cm of the measured voltage drop for the 4 h over which data were collected (Figure 8).

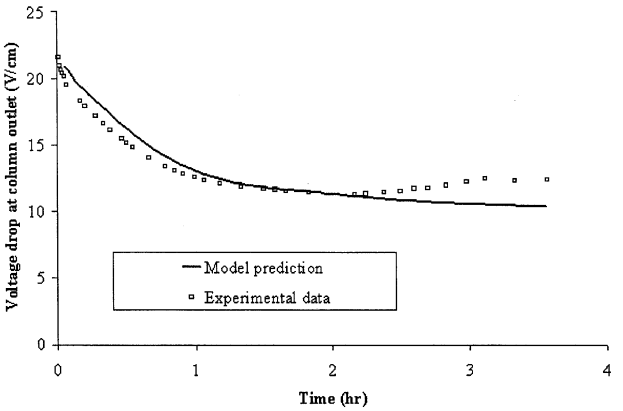

Figure 8. This model (Eq. 21) vs. experimental data for voltage drop at the column outlet.

Experimental and model conditions are identical to those in Figure 2(A).

Equivalent separations can be achieved upon scale-up by holding the column length constant while increasing the column diameter. Interstitial velocity, column length, voltage gradient, and current density are held constant so that heat generation per unit volume is also constant. As a result of increased total power generation and decreased heat removal from the external walls, the column temperature increases with increasing the diameters illustrated in Figure 7.

The model predicts that the maximum column diameter yielding separation of the proteins BSA and myoglobin shown in Figure 2B is 10.8 cm. Since the sample volume that can be processed during a single run in the same amount of time increases in proportion to the square of the column diameter, a sample size of 76.5 mL would be injected.

Column diameter also affects temperature and the average voltage gradient in the column. Conductivity increases and the resulting voltage gradient decreases when the center-line temperature increases. The average voltage gradient will decrease with increasing diameter since center-line temperature increases with increasing column diameters. Therefore, a perfectly cooled column that shows a lower temperature rise will result in a higher voltage gradient. Therefore, the resolution of the current equipment is expected to improve if a more thermally conductive column wall is found and enhanced cooling is achieved.

Conclusions

The model presented in this article accurately predicts the temperature rise for different cylindrical-column dimensions and two types of stationary phases. The electrical conductivity of the stationary phase, mobile phase, and the combination of the two are major contributors to heating characteristics. Therefore performance of the column is a function of both phases. However, the contribution of the liquid phase to thermal conductivity dominates that of the stationary phase. Hence, modeling of temperature profiles is based on the aqueous phase alone. The temperature dependence of the physical properties of water do not have a significant effect on the predicted temperature rise in the column. If 42°C is selected as a maximum operational temperature, the model predicts that scale-up of the current column to a diameter of 10.8 cm is possible, and processing of 75-mL sample volumes per run could be achieved.

Acknowledgments

This work was funded by an Andrews Fellowship from Purdue University, a Purdue University Research Fellowship, and Purdue University Agricultural Research Programs. The authors thank Kyle Beery, Nathan Mosier and Tom Huang from our laboratories for valuable comments and suggestions. We also thank Sheila Iuliano, Kevin O'Donnell, and Robert Picciotti from TosoHaas for technical information and the generous gift of the HW40-C stationary phase.

Notation

c_p = heat capacity, kJ/(kg·K)
d_p = particle diameter, m
D = column diameter, m
f_w = modified wall-corrected friction factor
g = gravitational acceleration, cm^2/s

h = heat-transfer coefficient, W/(m^2·K)
i_T = total current density, A/m^2
I = current, A
j = iteration counter
k = thermal conductivity, W/(m·K)
L = column length, m
M = wall-correction factor
Nu = Nusselt number
Pr = Prandtl number
Q = heat generation per unit volume, W/m^3
r = radial distance, m
R = column radius/inside radius of column wall, m
Ra_D = Rayleigh number
Re_d = particle Reynolds number
Re_D = column Reynolds number
Re_w = modified wall-corrected Reynolds number
R_w = outer radius of column wall, m
t = time, s
T = temperature, °C
u = superficial fluid velocity, m/s
x = column axial distance, m

Greek letters

α = thermal diffusivity, m^2/s
β = coefficient of thermal expansion, K^{-1}
ϵ_b = extraparticulate void fraction
ϵ_T = total void fraction
$d\Phi/dx$ = voltage gradient, V/m
κ = wall-corrected Kozeny–Carman factor
ν = kinematic fluid viscosity, m^2/s
ρ = density, kg/cm^3
σ = thermal capacity factor
σ_m = electrical conductivity of medium, (ohm·cm)$^{-1}$

Subscripts

a = air
f = properties of fluid used as mobile phase
forced = forced convection
free = free convection
i = inside column wall
init = initial condition
m = properties of packed-bed medium—includes both stationary- and mobile-phase properties
o = outside column wall
w = properties evaluated for plexiglass wall
r = at radial position r
ref = refrigeration
s = stationary phase—not including fluid inside

Literature Cited

Basak, S., A. Velayudhan, and M. R. Ladisch, "Characterization of Buffers for Electrokinetic Separations," *Appl. Biochem. Biotechnol.*, **44**, 243 (1994).

Basak, S., A. Velayudhan, K. Kohlmann, and M. R. Ladisch, "Electrochromatographic Separation of Proteins," *J. Chromatog. A*, **707**, 69 (1995).

Basak, S., and M. R. Ladisch, "Mechanistic Description and Experimental Studies of Electrochromatography of Proteins," *AIChE J.*, **41**(11), 2499 (1995).

Bejan, A., *Convection Heat Transfer*, 2nd ed., Wiley, New York, p. 523 (1995).

Bello, M. S., and P. G. Righetti, "Unsteady Heat Transfer in Capillary Zone Electrophoresis 1. A Mathematical Model," *J. Chromatog.*, **606**, 95 (1992).

Cole, K. D., and H. Cabezas, "Recent Progress in the Electrochromatography of Proteins," *Appl. Biochem. Biotechnol.*, **54**, 159 (1995).

Fand, R. M., and R. Thinakaran, "The Influence of the Wall on Flow Through Pipes Packed with Spheres," *J. Fluids Eng.—Trans. ASME*, **112**, 84 (1990).

Gobie, W., and C. Ivory, "Thermal Model of Capillary Electrophoresis and a Method for Counteracting Thermal Band Broadening," *J. Chromatog.*, **516**, 191 (1990).

Grushka, E., R. M. McCormick, and J. J. Kirkland, "Effect of Temperature Gradients on the Efficiency of Capillary Zone Electrophoresis Separations," *Anal. Chem.*, **61**, 241 (1989).

International Plastics Selector, 11th ed., D.A.T.A. Business Publishing, San Diego (1989).

Ivory, C., and W. Gobie, "Continuous Counteracting Chromatographic Electrophoresis," *Biotechnol. Prog.*, **6**, 21 (1990).

Keim, C., and M. Ladisch, "New System for Preparative Electrochromatography of Proteins," *Biotechnol. Bioeng.*, **70**, 72 (2000).

Krupiczka, R., "Analysis of Thermal Conductivity in Granular Materials," *Int. Chem. Eng.*, **7**, 122 (1967).

Lynch, E. D., and D. A. Saville, "Heat Transfer in the Thermal Entrance Region of an Internally Heated Flow," *Chem. Eng. Commun.*, **9**, 201 (1981).

Ostrach, S., "Convection in Continuous-Flow Electrophoresis," *J. Chromatog.*, **140**, 187 (1977).

Ozisik, M. N., *Heat Transfer: A Basic Approach*, McGraw-Hill, New York (1985).

Raj, C. B. C., and J. B. Hunter, "Analysis of Joule Heating in Electrophoretic Processes," *Int. Commun. Heat Mass Trans.*, **18**, 843 (1991).

Raj, C. B. C., "Preparative Electrophoresis—On the Estimation of Maximum Temperature," *Bioprocess. Eng.*, **11**, 65 (1994).

Rudge, S. R., S. K. Basak, and M. R. Ladisch, "Solute Retention in Electrochromatography by Electrically Induced Sorption," *AIChE J.*, **39**, 797 (1993).

Tiselius, A., "A New Apparatus for Electrophoretic Analysis of Colloidal Mixtures," *Trans. Faraday Soc.*, **33**, 524 (1937).

Turk, R. S., and C. F. Ivory, "Temperature Profiles in Plane Poiseuille Flow with Electrical Heat Generation," *Chem. Eng. Sci.*, **39**, 851 (1984).

Van Krevelen, D. W., *Properties of Polymers: Their Estimation and Correlation with Chemical Structure*, Elsevier, New York (1976).

Varahasamy, M., and R. M. Fand, "Heat Transfer by Forced Convection in Pipes Packed with Porous Media Whose Matrices are Composed of Spheres," *Int. J. Heat Mass Trans.*, **39**, 3931 (1996).

Vermuri, V., and W. J. Karplus, *Digital Computer Treatment of Partial Differential Equations*, Prentice-Hall, Englewood Cliffs, NJ (1981).

Manuscript received Aug. 4, 2000, and revision received July 12, 2002.